Journal of Electroanalytical Chemistry 660 (2011) 367–376

Contents lists available at ScienceDirect

Journal of Electroanalytical Chemistry

journal homepage: www.elsevier.com/locate/jelechem

Electric-field effects on the interfacial electron transfer and protein dynamics of cytochrome c

H. Khoa Ly [a], Nattawadee Wisitruangsakul [a,b], Murat Sezer [a], Jiu-Ju Feng [a,c], Anja Kranich [a], Inez M. Weidinger [a], Ingo Zebger [a], Daniel H. Murgida [d], Peter Hildebrandt [a,*]

[a] Technische Universität Berlin, Institut für Chemie, Sekr. PC 14, Straße des 17. Juni 135, D-10623 Berlin, Germany
[b] Iron and Steel Institute of Thailand, 1st-2nd Floor, Bureau of Industrial Sectors Development Building, Trimitr Soi., Pharam 4 Rd. Phakhanong, Klongtoey Bangkok 10110, Thailand
[c] School of Chemistry and Environmental Science, Henan Normal University, Xinxiang, Henan 453007, China
[d] Departamento de Química Inorgánica, Analítica y Química Física/INQUIMAE-CONICET, Facultad de Ciencias Exactas y Naturales, Universidad de Buenos Aires, Ciudad Universitaria, Pab. 2, Piso. 1, C1428EHA-Buenos Aires, Argentina

ARTICLE INFO

Article history:
Received 18 May 2010
Received in revised form 8 October 2010
Accepted 15 December 2010
Available online 21 December 2010

Keywords:
Surface enhanced Raman spectroscopy
Surface enhanced infrared spectroscopy
Electron transfer
Cytochrome c
Electric field

ABSTRACT

Time-resolved surface enhanced resonance Raman and surface enhanced infrared absorption spectroscopy have been employed to study the interfacial redox process of cytochrome *c* (Cyt-c) immobilised on various metal electrodes coated with self-assembled monolayers (SAMs) of carboxyl-terminated mercaptanes. The experiments, carried out with Ag, Au and layered Au–SAM–Ag electrodes, afford apparent heterogeneous electron transfer constants (k_{relax}) that reflect the interplay between electron tunnelling, redox-linked protein structural changes, protein re-orientation, and hydrogen bond re-arrangements in the protein and in the protein/SAM interface. It is shown that the individual processes are affected by the interfacial electric field strength that increases with decreasing thickness of the SAM and increasing difference between the actual potential and the potential of zero-charge. At thick SAMs of mercaptanes including 15 methylene groups, electron tunnelling (k_{ET}) is the rate-limiting step. Pronounced differences for k_{ET} and its overpotential-dependence are observed for the three metal electrodes and can be attributed to the different electric-field effects on the free-energy term controlling the tunnelling rate. With decreasing SAM thickness, electron tunnelling increases whereas protein dynamics is slowed down such that for SAMs including less than 10 methylene groups, protein re-orientation becomes rate-limiting, as reflected by the viscosity dependence of k_{relax}. Upon decreasing the SAM thickness from 5 to 1 methylene group, an additional H/D kinetic isotope effect is detected indicating that at very high electric fields re-arrangements of the interfacial or intra-protein hydrogen bond networks limit the rate of the overall redox process.

1. Introduction

Interfacial electron transfer (ET) reactions play a key role in various processes of technological importance such as catalysis, corrosion and energy conversion or storage [1–3]. Furthermore, they are constitutive for a large number of biological functions and essential for most of the biotechnological applications that utilize redox enzymes [4]. This wide range of fundamental and applied aspects of heterogeneous ET has motivated numerous experimental and theoretical studies for decades. It is, therefore, quite surprising that these elementary reactions are yet not comprehensively understood.

One reason for this quite remarkable gap is related to methodological shortcomings. For a long time, electrochemical methods have been the only techniques for determining thermodynamic and kinetic data of redox processes although the nature of the participating molecules could not be directly identified [5,6]. Thus, analyses of mechanistic aspects of interfacial redox processes had to rely upon indirect evidences.

In this respect, surface enhanced Raman (SER) and surface enhanced infrared absorption (SEIRA) spectroscopy represent powerful complementary techniques since the vibrational spectra of molecules in close vicinity of metal electrodes can be selectively probed due to the resonant coupling of the radiation field with the surface plasmons of the metallic support, which may be Ag or Au [7,8]. These methods can be coupled with the potential jump technique such that they provide information of the kinetics and thermodynamics of the interfacial processes and the nature of the molecule species involved [9–13].

SER and SEIRA spectroscopy have been employed to study interfacial processes of redox proteins [14–17]. In these studies, the SER

* Corresponding author. Tel.: +49 30 314 21419; fax: +49 30 314 21122.
E-mail address: hildebrandt@chem.tu-berlin.de (P. Hildebrandt).

1572-6657/$ - see front matter © 2010 Elsevier B.V. All rights reserved.
doi:10.1016/j.jelechem.2010.12.020

effect is combined with the molecular resonance Raman (RR) effect (surface enhanced resonance Raman – SERR) such that it is possible to selectively probe the redox site solely of the immobilised proteins by tuning the excitation line in resonance with both the electronic transition of the cofactor *and* the surface plasmons of the metal [7,8]. The sensitivity and selectivity of SEIRA spectroscopy is increased upon operating in the difference mode such that only potential-dependent changes of the vibrational bands of the protein *and* the cofactor are detected [13,16,17].

A widely used model system, appropriate for employing SERR and SEIRA spectroscopy as well as electrochemical methods, is based on Au or Ag electrodes coated by self-assembled monolayers (SAM) of mercaptanes [14,15]. Such coatings on Au surfaces have been first characterised by Nuzzo and Allara [18] and later used for biocompatible immobilisation of redox proteins [19–21]. The terminal tail groups of the mercaptanes can be varied to allow for different modes of protein binding and the thickness of the SAM is defined by the number of methylene groups in the alkyl chain of the mercaptanes. These devices allow systematic variation of important parameters controlling the heterogeneous ET, such as the ET distance, driving force, charge distribution in the SAM/protein interface, and ionic strength, viscosity, and pH in the bulk solution.

A particularly large body of experimental and theoretical data has been accumulated for the redox process of the heme protein cytochrome *c* (Cyt-c) electrostatically immobilised on electrodes coated with carboxyl-terminated SAMs [11–17,20–50]. The results obtained so far indicate that the overall redox process is determined by the coupling of protein dynamics with electron tunnelling [42,46–48]. This coupling results from the fact that the energetically preferred electrostatic binding domain corresponds to an orientation of the bound protein that exhibits a distinctly lower tunnelling probability than a lower affinity binding site [46,48]. Optimum electron tunnelling efficiency, therefore, requires rotational motions of the protein on the SAM. This conclusion seems to provide a satisfactory explanation for the unique distance-dependence of the experimentally observed ET rate which first increases exponentially with decreasing distance, i.e. the SAM thickness, but then levels off to a plateau region for SAMs shorter than 10 methylene groups [12–15,23,25,27,29–32,42]. This region has, hence, been attributed to a kinetic regime in which protein-re-orientation becomes the rate-limiting step [42]. This interpretation is consistent with the experimental finding that the relaxation constants for protein re-orientation decrease substantially with decreasing distance in contrast to the exponential increase of the electron tunnelling rate. The slow-down of the protein dynamics with decreasing distance has been attributed to the concomitant increase of the electric field strength at Cyt-c/SAM interface, thereby increasing the activation energy for protein re-orientation. Thus, the interfacial redox process *in toto* has been suggested to be modulated by the electric field. Evidently, this scenario holds for quite different proteins which have been shown to exhibit a similar non-exponential distance dependence of the heterogeneous ET rate constant [51–55].

However, there are still some observations which do not fully fit into this scheme. First, in the limit of highly restricted protein mobility, one would expect at least a slight increase of the ET rate with further decreasing the electron tunnelling distance due to the exponential increase of the electronic coupling parameter in each protein orientation. However, all experimental data reported so far indicate an essentially distance-independent regime for short distances, i.e. high electric fields. Second, although experimental data obtained for SAM-coated Au and Ag electrodes display a qualitatively similar distance dependence, even for the same protein (i.e. Cyt-c) the absolute values for the experimentally determined ET rate constants are generally higher for Au than for Ag [12,13,23,25,27–29,36,38,45]. Third, in the plateau region, the ET rate constants have been shown to be lower in D_2O compared to H_2O, which has been ascribed to a kinetic isotope effect due to the coupling of electron transfer with redox-linked proton translocation in the protein or in the protein/SAM interface [12,43]. Although recently a part of this isotope effect was attributed to the intrinsically higher viscosity of D_2O solutions [43], it remains to be clarified why the ratio of the rate constants in H_2O and D_2O increases with decreasing distance to the electrode.

In the present work we have addressed these three questions by employing time-resolved (TR) SERR and SEIRA spectroscopy to probe the distance- and overpotential-dependence of the interfacial ET on Ag, Au, and Au–SAM–Ag hybrid electrodes. Special emphasis is laid on the analysis of viscosity and H/D effects on the kinetic constants. The results lead to the conclusion that not only protein re-orientation but also the electron tunnelling step itself is controlled by the interfacial electric field.

2. Experimental

2.1. Materials

6-mercaptohexanoic acid (C_5) from Dojindo, 16-mercaptohexadecanoic acid (C_{15}), 11-mercaptoundecanoic acid (C_{10}), and mercaptoacetic acid (C_1), all purchased from Sigma–Aldrich, were used without further purification. Formation of SAMs on the metal electrode followed the protocol described previously [26]. Horse heart Cyt-c from Sigma–Aldrich was purified by HPLC. The water used in all experiments was purified by a Millipore system and its resistance was more than 18 MΩ. All other chemicals were of highest purity grade available.

2.2. Surface Enhanced Resonance Raman spectroscopy

The spectroelectrochemical cell for SERR spectrosocpy has been described elsewhere [26]. All potentials cited in this work refer to the Ag/AgCl (3 M KCl) electrode. A rotating Ag ring served as the working electrode. SER-activation, coating of the electrode by SAMs and subsequent protein immobilization followed the protocol described previously with minor modifications [10,26]. Briefly, prior to the spectroscopic experiments, the electrolyte solution (30 mM phosphate buffer, pH = 7.0) was bubbled with catalytically purified oxygen-free argon for ca. 20 min. Consecutively, Cyt-c solution was added yielding a final concentration of ca. 0.2 μM. Protein adsorption was achieved by incubating the working electrode for 30 min into the protein containing buffer solution at open circuit potential. All experiments were performed in the presence of protein in solution and Ar overpressure.

For experiments in D_2O, the protein was dissolved in buffered D_2O solutions adjusted to pD = 7.0 [12] and subsequently incubated for further 18–24 h for complete H/D exchange. To account for the intrinsically higher viscosity of D_2O, comparative experiments in H_2O buffer were carried out at a viscosity of 1.2 cp adjusted by addition of sucrose [42]. All SERR measurements were carried out with a roughened Ag electrode [10] or an Au–SAM–Ag electrode fabricated as described previously [45].

SERR spectra were measured in back-scattering geometry using a confocal microscope coupled to a single stage spectrograph (Jobin Yvon, LabRam 800 HR) equipped with a liquid-nitrogen cooled back illuminated CCD detector. The 413-nm line of a cw Krypton ion laser (Coherent Innova 300c) was focused onto the surface of the rotating Ag electrode by means of a long working distance objective (20×; NA 0.35). Typically, experiments were performed with laser powers of ca. 1 mW. Effective acquisition times were between 3 and 10 s. All experiments were repeated several times to

ensure reproducibility. For TR-SERR experiments, potential jumps of variable height and duration were applied to trigger the reaction. The SERR spectra were measured at different delay times following the potential jump. Further details of the stationary and TR-SERR experiments are given elsewhere [11,15,27]. After background subtraction the spectra were treated by a component analysis in which the spectra of the individual species were fitted to the measured spectra using a home-made analysis software [56,57].

2.3. Surface enhanced infrared absorption measurements

SEIRA measurements were performed with a Kretschmann-ATR configuration using a semi-cylindrical shaped silicon crystal. Thin gold (Au) films were formed on the flat surface of the silicon substrate by electroless (chemical) deposition technique [13]. For Cyt-c adsorption, SAM-coated electrodes were immersed in Cyt-c solution using a concentration of 2 μM. The SEIRA spectra were recorded from 4000 to 1000 cm^{-1} with a spectral resolution of 4 cm^{-1} on a Bruker IFS66v/s spectrometer equipped with a photoconductive MCT detector. Four hundred scans were co-added for a spectrum. For the spectro-electrochemical measurements, the ATR crystal was incorporated into a three-electrode home-built cell [13].

TR SEIRA experiments were carried out using the potential jump technique [13]. Spectra acquisition was synchronized with the potential jumps controlled by a home-made pulse delay generator. Series of time dependent single-channel spectra of Cyt-c were collected when a potential jump was carried out from the reference potential at which Cyt-c was either largely reduced (−0.1 V) or oxidised (+0.125 V) to the final potential, and for the reverse jump. Depending on the time scale under examination, either step-scan or rapid-scan TR SEIRA measurements were carried out. The photoconductive MCT detector with a fast amplifier was used in the DC-coupled mode for the step-scan measurements. In the case of the rapid-scan measurements, the AC-coupled mode was utilized. Details of the set-up as well as of the stationary and TR SEIRA experiments have been described previously [13].

3. Results

3.1. Stationary SERR spectra and spectra analysis

SERR spectra of Cyt-c were measured from Ag electrodes coated with carboxyl-terminated thiols of different chain lengths (C_x-SAM), expressed by the number of methylene groups *x*. For chain lengths with $x = 15$, 10, 5, SERR spectra do not provide any indication for contributions from species other than the native state (denoted as B1). Thus, these spectra could be well described by a superposition of the reduced and oxidised forms of state B1 using component analysis. For shorter SAMs, however, there are non-negligible contributions from non-native species (denoted as state B2) which increase upon approaching potentials above the redox potential of the native state [57,58], as reflected, *inter alia*, by a broadening of the peaks in the ν_4 and ν_3 band region (Fig. 1). These species include a five-coordinated high spin (5cHS) and a six-coordinated low spin (6cLS) ferric heme in which the native Met80 ligand is removed from the heme iron and this coordination site remains vacant or is replaced by a His, respectively [57]. The formation of these species is most likely related to the weakening of the Fe-Met80 bond of native ferric Cyt-c (B1) by the high electric fields in close proximity to the electrode as concluded from previous experimental and theoretical studies [57–59]. Thus, the analysis of the SERR spectra measured under these conditions has to consider the involvement of four different species, i.e., $B1_{red}$, $B1_{ox}$, $B2_{ox}$ [5cHS], and $B2_{ox}$ [6cLS]. Then, the

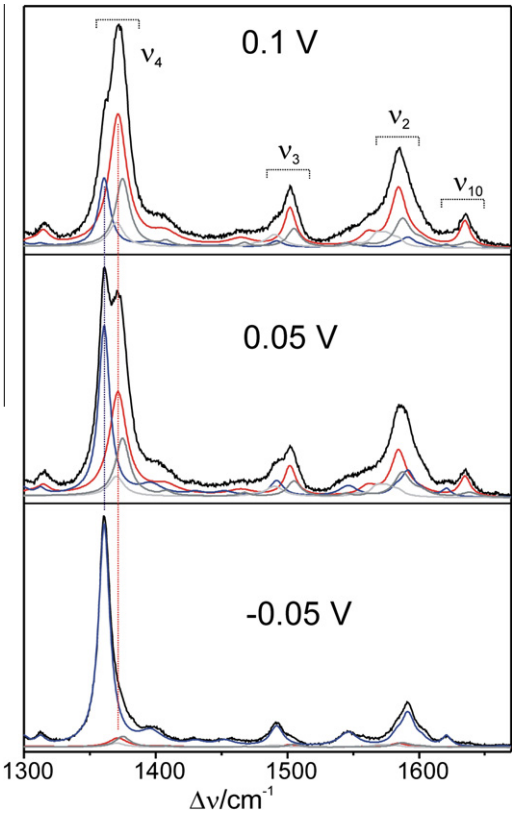

Fig. 1. SERR spectra of Cyt-c immobilised on a C_1-SAM-coated Ag electrode at different electrode potentials. The blue, red, dark gray, and light gray lines represent the component spectra of the reduced B1, oxidised B1, oxidised B2[6cLS], and oxidised B2[5cHS] state, respectively. Further experimental details are given in the text. (For interpretation of the references to colour in this figure legend, the reader is referred to the web version of this article.)

component analysis provides a consistent description of all experimental spectra, yielding the relative spectral contributions of each component to the individual experimental spectra. These spectral contributions were subsequently converted to relative concentrations [57]. The results of the analysis of the SERR spectra of Cyt-c at a C_1-SAM-coated Ag electrode, measured as a function of the electrode potential, are shown in Fig. 2. The only redox transition refers to the native state B1 as demonstrated by a fit of the Nernstian equation to the data, allowing for the determination of the redox potential E^0 and the number of transferred electrons *n* (Table 1). No effect on the redox equilibrium was observed upon increasing the viscosity of the solution or upon H/D exchange.

The non-native species are only present in the oxidised forms. The corresponding reduced counterparts are formed with electrode potentials below −0.3 V and are then rapidly converted to the native reduced B1 state [58,60], such that they are not detectable under equilibrium conditions in the stationary measurements.

3.2. Distance-dependence of the apparent electron transfer rate constant

TR-SERR experiments were first performed employing potential jumps from negative potentials (−0.1 V) to the redox potential such that relaxation processes include the ET of the immobilised Cyt-c at zero-driving force ($\Delta G = 0$ eV). These experiments were carried out as a function of the SAM thickness for $x = 15$, 10, 5, and 1 on Ag electrodes. As in the stationary experiments, spectra for $x \geqslant 5$ only include the native species whereas at $x = 1$ also the component spectra of the two B2 species were required for a

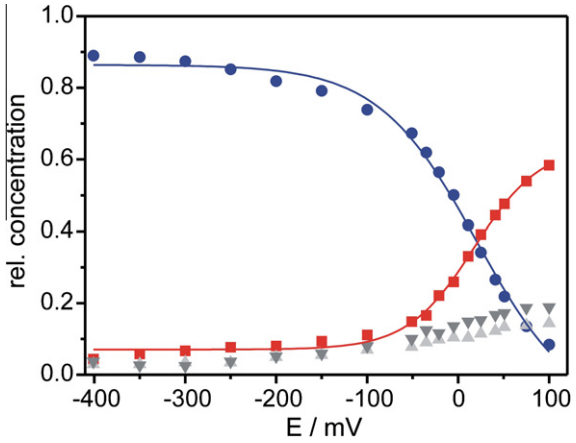

Fig. 2. Potential-dependent distribution of the relative concentrations of the various species of Cyt-c immobilised on a C_1-SAM-coated Ag electrode, as determined by SERR spectroscopy. The blue(circles), red(squares), dark gray(down-pointing triangle), and light gray(up-pointing triangle) symbols represent the reduced B1, oxidised B1, oxidised B2[6cLS], and oxidised B2[5cHS] state, respectively. The solid lines refer to a fit of the Nernst equation to the experimental data. Further experimental details are given in the text. (For interpretation of the references to colour in this figure legend, the reader is referred to the web version of this article.)

Table 1
Redox potentials and relaxation constants at zero-driving force for the interfacial redox process of Cyt-c immobilised on Ag electrodes coated with different SAMs.[a]

SAM	Buffer	E^0 (V)	k_{relax} (s^{-1})
C_{10}	H_2O	0.021	53
	H_2O, 1.2 cp	0.019	45
	D_2O	0.020	48
C_5	H_2O	0.018	130
	H_2O, 1.2 cp	0.010	100
	D_2O	0.015	100
C_1	H_2O	0.033	40
	H_2O, 1.2 cp	0.031	30
	D_2O	0.030	16

[a] The data were obtained by TR-SERR experiments with potential jumps from −0.1 V to the redox potential. The average error associated with the determination of E^0 and k_{relax} was determined to be ±005 V and ±10%.

satisfactory global fit to the experimental TR SERR spectra. Representative example spectra of experiments with Cyt-c on a C_1-SAM-coated Ag electrode are shown in Fig. 3. The time-dependent relative concentration changes of the various species indicate a clear correlation between the decay of the reduced and the increase of the oxidised B1 state (Fig. 4). The non-native species initially grow in and then reach a constant level after ca. 20 ms. Thus, the kinetic analysis cannot be restricted to the redox process of the native state but must also include the formation of the B2 species. A qualitatively similar kinetic behaviour has been recently observed for Cyt-c covalently attached to SAM-coated Ag electrodes, and found to be adequately described by the scheme in which $B1_{ox}$ exhibits a reaction channel to $B2_{ox}$[5cHS] in equilibrium with $B2_{ox}$[6cLS] [47]. In a similar way, we have considered the temporal evolution of the B2 species in the present kinetic analysis which thus allowed determining the relaxation constant k_{relax} of the redox process of B1 (Table 1).

For the C_{15}-SAM, k_{relax} was identical to the previously determined value [12] but with decreasing chain length the relaxation constants obtained in this work were found to be smaller than the constants reported earlier, specifically for the C_1-SAM. As a consequence, the distance-dependence of k_{relax} does not display a plateau for $x < 10$ but even a decrease at $x < 5$ (Fig. 5).

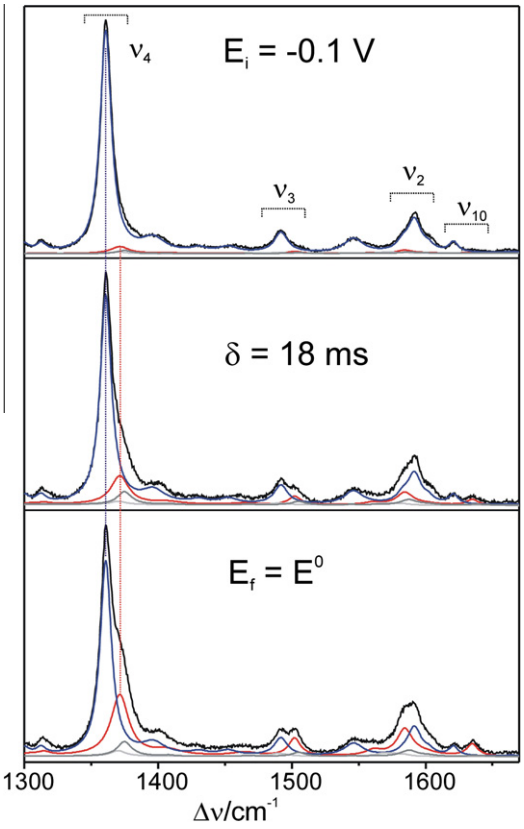

Fig. 3. Selection of SERR spectra of a time-resolved experiment of Cyt-c immobilised on a C_1-SAM-coated Ag electrode, including the stationary SERR spectra at the initial potential $E_i = -0.1$ V and the final potential $E_i = E^0$, and a TR SERR spectrum obtained after a delay time $\delta = 18$ ms subsequent to the potential jump. The blue, red, dark gray, and light gray lines represent the component spectra of the reduced B1, oxidised B1, oxidised B2[6cLS], and oxidised B2[5cHS] state, respectively. Further experimental details are given in the text. (For interpretation of the references to colour in this figure legend, the reader is referred to the web version of this article.)

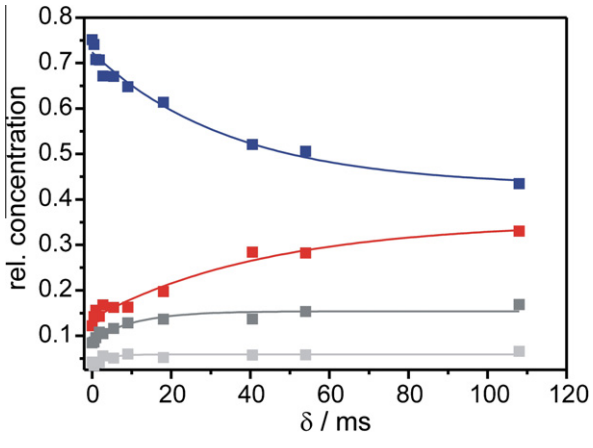

Fig. 4. Time-dependent changes of the relative concentrations of the various species of Cyt-c immobilised on a C_1-SAM-coated Ag electrode, following a potential jump from $E_i = -0.1$ V to the $E_i = E^0$. The experimental data were determined by TR SERR spectroscopy. The blue, red, dark gray, and light gray symbols represent the reduced B1, oxidised B1, oxidised B2[6cLS], and oxidised B2[5cHS] state, respectively. The solid lines refer to a fit of exponentials to the experimental data. Further details of the experiments and the data analysis are given in the text. (For interpretation of the references to colour in this figure legend, the reader is referred to the web version of this article.)

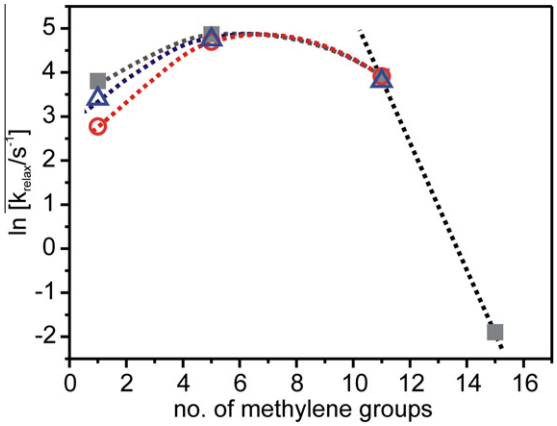

Fig. 5. Relaxation constants for the interfacial redox process of Cyt-c at zero-driving force at Ag electrodes coated with SAMs of different thickness, expressed by the number of methylene groups. The solid squares (dark gray), open triangles (blue), and open circles (red) symbols refer to the data obtained in H_2O, H_2O/sucrose (1.2 cp), and D_2O buffer, respectively. The dotted lines are just to guide the eye. Further details of the experiments and the data analysis are given in the text. (For interpretation of the references to colour in this figure legend, the reader is referred to the web version of this article.)

3.3. Kinetic isotope and viscosity effects of the apparent electron transfer rate constant

Preliminary SEIRA experiments monitoring the amide I band changes indicated that a complete H/D exchange requires incubation times for more than 24 h which is consistent with previous studies revealing a wide dynamic range for the substitution of the exchangeable protons [61,62]. Here we have chosen two different protocols for the H/D exchange. First, ferric Cyt-c was incubated in D_2O buffer solutions (pD 7.0) for different periods of time from 1 h to 24 h. Second, to achieve an exchange of protons that are hardly accessible in the folded form, the protein was first unfolded in the presence of GuHCl at pH 2.0 in D_2O and subsequently refolded in neutral (buffered) D_2O solution [63]. However, in all cases, the kinetic constants, determined for a potential jump to the redox potential at a given SAM by SERR spectroscopy, were found to be the same.

TR-SERR experiments on Ag electrodes coated with SAMs with $x \geqslant 10$ in D_2O afforded relaxation constants equal to those determined in H_2O whereas for C_5-SAM-coated Ag electrode, the experiments yielded a 1.3 times smaller value in D_2O (Table 1). At C_1-SAM, the relaxation constant was found to be smaller by a factor of 2.5 as compared to the value in H_2O. Next, we carried out distance-dependent TR SERR measurements in H_2O buffer solution including 6.5% sucrose to match the viscosity of D_2O. Again, no changes of the relaxation constants were noted at long chain lengths whereas at C_5-SAM a value of 100 s^{-1} was determined that is smaller by a factor of 1.3 than in H_2O buffer in the absence of sucrose. The same ratio of the relaxation constants was found for C_1-SAM in the presence and in the absence of sucrose.

On the other hand, step-scan SEIRA experiments on C_5-SAM-coated Au electrodes afford a value for k_{relax} of 800 s^{-1} that does not exhibit H/D or viscosity sensitivity within the experimental error of 10%.

3.4. Overpotential-dependence of the heterogeneous electron transfer rate constant

The relaxation constants of the interfacial redox process of Cyt-c, k_{relax}, were determined as a function of the overpotential for C_{15}-SAM-coated electrodes in H_2O buffer. Here, we have employed potential jumps from an initial potential $E_i \geqslant E^0$ to a final potential $E_f < E^0$ such that the amount of the overpotential $\eta = E_f - E^0$ was stepwise increased. Such measurements have been previously carried out with Cyt-c immobilised on SAM-coated Ag electrodes (Table 2) [27]. In this work, we have extended the experiments to C_{15}-SAM-coated Au and Au–SAM–Ag hybrid electrodes, probing the relaxation process by rapid-scan SEIRA and TR SERR spectroscopy, respectively. SEIRA spectroscopy allows monitoring the redox process of the immobilised Cyt-c on the basis of various redox-sensitive amide I bands at 1693 and 1673 cm^{-1} which have been assigned to the β-turn type III segment 67–70 of the reduced and oxidised Cyt-c, respectively (Figs. 6 and 7) [13]. For zero-driving force ($\eta = 0$ V), k_{relax} was determined to be 0.29 s^{-1} using the average of the relaxation constants derived from the intensity changes of the individual redox-sensitive amide bands (Table 2). This value is by a factor of 2 larger than the corresponding value determined for Ag electrodes under otherwise identical conditions. Increasing the driving force, however, leads to a much smaller increase of k_{relax} as compared to the C_{15}-SAM-coated Ag electrode with 0.35 and 0.77 s^{-1} at $\eta = -0.24$ V and $\eta = -0.44$ V, respectively. A further increase of the driving force ($\eta = -0.49$ V) causes only a slight increase of k_{relax} (Table 2). These observations are in sharp contrast to the results obtained for the C_{15}-SAM-coated Ag electrode for which a substantially larger overpotential-dependent increase of k_{relax} was noted [27].

A comparably unprecedented behaviour is found for the Au–SAM–Ag hybrid electrode [45,50]. This device is based on an electrochemically roughened Ag electrode, coated by a SAM of 11-amino-1-undecanethiol (AUT) which in turn is covered by a 15-nm thick Au film. The Au surface is then functionalised by a (carboxyl-terminated) C_{15}-SAM to allow for Cyt-c binding. The hybrid electrodes offer the advantage of combining the optical properties of Ag with the electrochemical stability of Au [45]. Moreover, the dielectric spacer between the two metals promotes plasmon excitation such that the intensity of the SERR spectrum of Cyt-c immobilised on the outer C_{15}-SAM layer of the Au film is comparable to that observed for Cyt-c at C_{15}-SAM Ag electrodes. The SERR spectra with 413-nm excitation afford qualitatively the same results as observed for the Ag-only electrode system, i.e. with no contribution from non-native species at long chain lengths [45,50]. ET of the immobilised Cyt-c on C_{15}-SAM-coated

Table 2
Relaxation constants for the interfacial redox process as a function of the overpotential of Cyt-c immobilised on different electrode systems.[a]

SAM	Ag (SERR)[b]		Au (SEIRA)		Au–SAM–Ag (SERR)	
	$-\eta$ (V)	k_{relax} (s^{-1})	$-\eta$ (V)	k_{relax} (s^{-1})	$-\eta$ (V)	k_{relax} (s^{-1})
C_{15}	0	0.15	0	0.29	0	0.77
	−0.05	0.26			−0.05	1.2
	−0.1	0.60			0.1	1.2
	−0.13	0.80				
	−0.2	1.5	−0.24	0.35	−0.2	4.9
	−0.3	2.88			−0.3	8.2
	−0.4	3.73	−0.44	0.77	−0.45	9.0
	−0.6	3.91	−0.49	0.83	−0.5	9.6
C_{10}	0	53	0	72	0	45
	−0.19	240				
	−0.22	320	−0.25	180	−0.2	167
	−0.29	370				
	−0.39	500			−0.4	313
	−0.44	550				

[a] The data were obtained by TR-SERR experiments with potential jumps from +0.1 V to different final potentials E_f corresponding to an overpotential of $\eta = E_f - E^0$. The average error associated with the determination of k_{relax} was ±10%. The k_{ET} values for Cyt-c on C_{15}-SAM-coated electrodes as discussed in the text were calculated according to Eq. (2).

[b] Data taken from Refs. [27,42].

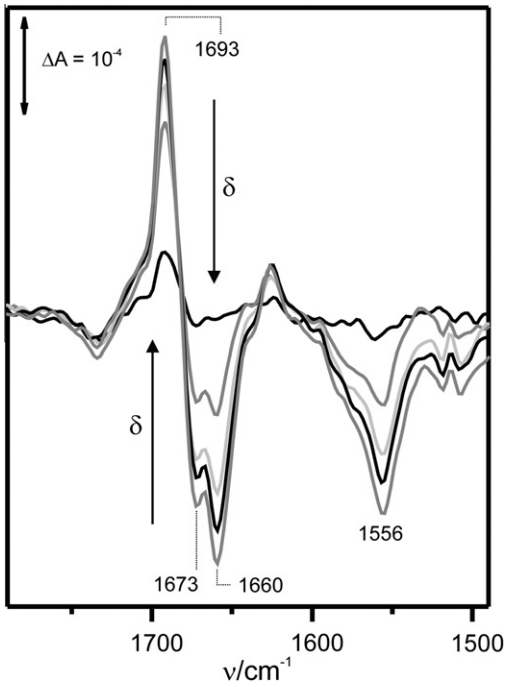

Fig. 6. Rapid scan SEIRA difference spectra of Cyt-c immobilised on a C_{15}-SAM-coated Au electrode for a potential jump from +0.125 V to −0.4 V. The reference spectrum refers to the initial potential of +0.125 V. The individual spectra that are displayed refer to delay times of 0.5, 1, 2.5, 5, and 15 s. The solid arrows indicate the direction of increasing delay times. Further details of the experiments are given in the text.

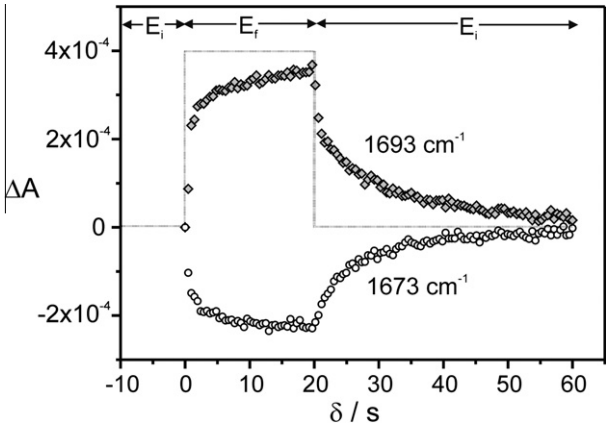

Fig. 7. Time-dependent changes of the intensities of the 1693 and 1673-cm^{-1} bands determined from rapid-scan SEIRA difference spectroscopy of Cyt-c on C_{15}-SAM-coated Au electrode. The data were obtained from potential jump experiments from +0.125 V (E_i) to −0.4 V (E_f). The reference spectrum refers to the initial potential of +0.125 V. Further details of the experiments are given in the text.

Au–SAM–Ag electrodes proceeds via different regimes. For the oxidation reaction, the first step is electron tunnelling from Cyt-c through the outer C_{15}-SAM coating to the Au film, followed by metallic conductance across the Au film in the second step, and, in the third step, again by electron tunnelling through the AUT SAM to the Ag electrode. The electron transport through the metallic Au film is much faster than the tunnelling processes for which the rates depend on the thickness of the respective SAMs. Thus, one intuitively expects that the ultimate rate-limiting step is tunnelling through the outer C_{15}-SAM coating. This conclusion is in fact confirmed by a recent systematic analysis of the ET processes of Cyt-c at C_x-SAM-coated Au–SAM–Ag devices in which the thickness of the inner and the outer SAMs was varied [50]. Consequently, we can compare the ET dynamics of Cyt-c on C_{15}-SAM-coated Au–SAM–Ag electrodes directly with those at C_{15}-SAM-coated Au and Ag electrodes. In this respect, the experimentally determined rate constant is found to be higher by a factor of ca. 2.6 and 5.1 than for the Au and Ag electrode system, respectively. However, the overpotential is weaker than for Ag albeit more pronounced than for Au (Table 2).

Analogous experiments were carried out with Cyt-c immobilised on C_{10}-SAM coatings for all three electrode systems. The corresponding values for k_{relax} are listed in Table 2.

4. Discussion

Electrostatic binding of Cyt-c to electrodes coated with carboxyl-terminated SAMs proceeds mainly via two binding domains [46,48]. The high affinity domain (BD3), involving the lysine residues 72, 73, 79, 86, and 87, is, however, associated with a distinctly lower average electron tunnelling probability than the medium-affinity binding domain (BD2), defined by lysine residues 25 and 27. Thus, optimum electron tunnelling requires the rotational diffusion of the immobilised Cyt-c, which at C_{15}-SAM-coated Ag electrodes proceeds with the rate constant k_{orient} larger than 6000 s^{-1} as determined by TR SERR spectroscopy with 514 nm excitation [42]. This approach is based on the orientation-dependent preferential enhancement of heme modes of different symmetry under Q-band excitation. In contrast, the kinetic data obtained by TR SERR spectroscopy with 413-nm (Soret band) excitation as used in this work represent relaxation constants k_{relax} describing the reduction and oxidation of the heme. The latter experiments afford the relaxation of the individual oxidised and reduced Cyt-c species A_i following a potential jump. This relaxation is generally described by a mono-exponential function

$$A_i(\delta) = A_i(E_i) \cdot \exp(-k_{relax} \cdot \delta) \quad (1)$$

where $A_i(\delta)$ and $A_i(E_i)$ are the concentration of the species under consideration at the delay time δ and at the initial potential E_i (δ = 0 s). For C_{15}-SAM-coated Ag electrodes, k_{relax} is 0.15 s^{-1} at zero-driving force and it increases to nearly 4 s^{-1} upon raising the modulus of the overpotential [27]. Thus, k_{orient} is always distinctly larger than k_{relax} implying that at C_{15}-SAM-coated Ag electrodes the TR-SERR experiments directly probe electron tunnelling. In a first approximation, this is also true for C_{10}-SAM coatings where, at zero-deriving force, k_{relax} is ca. 50 s^{-1} compared to k_{orient} = 390 s^{-1} [42]. However, with increasing driving force, k_{relax} approaches k_{orient} which becomes the limiting value of the overpotential-dependence of k_{relax}. For C_5-SAM coatings, even at zero-driving force, the same values were determined for k_{relax} and k_{orient} [42]. Under these conditions, the overall kinetics of the interfacial ET is the result of the convolution of protein dynamics and electron tunnelling and should, in fact, follow a more complex kinetic behaviour that deviates from a mono-exponential decay [49]. However, within the experimental accuracy and due to the limited time-resolution of the TR-SERR experiments, the description of the relaxation processes does not justify fit functions that are more complex than a single exponential.

On the other hand, the increasing deviations for the values of k_{relax} for C_x-SAM coatings with $x \leqslant 10$ determined in this work and those obtained earlier in our group (Table 2, [12]) may be related to the fact that the mono-exponential approximation becomes less accurate for thinner SAM coatings. In contrast to the fit of Eq. (1) to the data in this work, we have previously employed a fit of the linearized Eq. (1) [12], which might overestimate fast events in the case of a complex kinetic behaviour. As a consequence, the previous study afforded increasingly larger k_{relax} values for C_x-SAM coatings with $x \leqslant 10$, compared to the present results.

In addition, the present spectra analysis is not restricted to the ν_4 and ν_3 band region as previously [12] but covers a wider spectral range, thereby increasing the accuracy specifically for thinner SAMs where contributions from the non-native states gain importance. This different spectra analysis may also account for the slight differences of the redox potentials determined from stationary SERR experiments (Table 1, [26]).

4.1. Electric-field effects on electron tunnelling

At C_{15}-SAM-coated Ag electrodes, i.e. in the tunnelling regime, k_{relax} determined from the TR-SERR experiments is related to the electron tunnelling rate constant k_{ET} for the reduction of the heme according to

$$k_{ET} = \frac{k_{relax} \cdot K_{eq}}{(1 + K_{eq})} \tag{2}$$

where K_{eq} is the redox equilibrium constant

$$K_{eq} = \exp\left(-\frac{(E - E^0) \cdot n \cdot e}{k_B T}\right) \tag{3}$$

with E, e, k_B, and T denoting the electrode potential, the elementary charge, the Boltzmann constant, and the temperature, respectively. Thus, for zero-driving force corresponding to $\eta = E - E^0 = 0$ V, we obtain $k_{ET} = 2k_{relax}$.

Eqs. (2) and (3) also hold for the relaxation constants derived from the mono-exponential fits to intensity changes of the SEIRA bands at 1693 and 1673 cm^{-1} measured for Cyt-c on C_{15}-SAM-coated Au electrodes, since these changes seem to proceed instantaneously with the heterogeneous ET [13]. This conclusion is very plausible as the amide I band changes most likely reflect the redox-linked protein structural changes, i.e. the protein reorganisation, which occurs much faster than long-distance electron tunnelling considered in this work. Furthermore, even for C_5-SAM-coated Au electrodes, k_{relax} at zero-driving force was found to be unaffected by an increase of the viscosity to 1.2 cp, implying that protein reorientation is faster than electron tunnelling. Thus, we can safely conclude for both the Ag and the Au electrode, the C_{15}-SAM coating refers to a regime, in which, regardless of the overpotential, electron tunnelling is the rate-limiting step. The same considerations hold for the Au–SAM–Ag electrode.

Electron tunnelling between an immobilised redox site and the electrode can be described according to Eq. (4) [64,65]

$$k_{ET}(\eta) \approx \frac{\pi}{\hbar} \cdot |V|^2 \cdot \rho \cdot \exp(-\beta \cdot d) \cdot erfc\left(\frac{\lambda + e\eta}{\sqrt{4\lambda k_B T}}\right) \tag{4}$$

where λ, V, and ρ are the reorganisation energy, the electronic coupling parameter, and the density of states in the electrode, respectively, and $erfc(z)$ is the complementary error function. The exponential function in Eq. (4) represents the distance-dependence of the electronic coupling parameter with d and β denoting the ET distance and the tunnelling decay parameter. Upon relating the ET rate constant at a given overpotential $k_{ET}(\eta)$ with the rate constant at zero-driving force ($\eta = 0$ V), $k_{ET}(0)$, one obtains

$$\frac{k_{ET}(\eta)}{k_{ET}(0)} = \frac{erfc\left(\frac{\lambda + e\eta}{\sqrt{4\lambda k_B T}}\right)}{erfc\left(\frac{\lambda}{\sqrt{4\lambda k_B T}}\right)} \tag{5}$$

which has been employed to determine the reorganisation energy for the electron tunnelling process of Cyt-c immobilised on a C_{15}-SAM-coated Ag electrode (Fig. 8) [27]. In this way, a reorganisation of 0.22 eV has been determined.

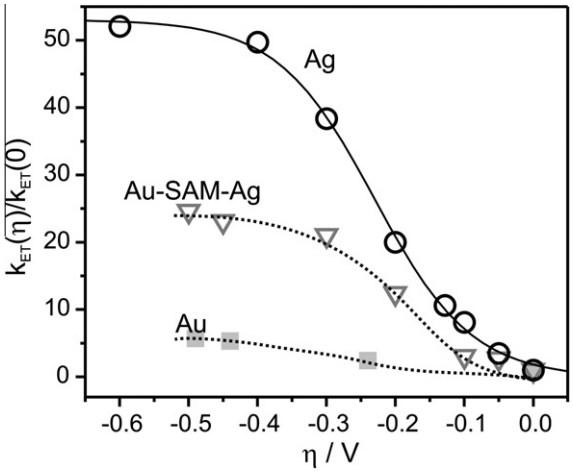

Fig. 8. Overpotential-dependence of the heterogeneous electron transfer rate constant k_{ET} for Cyt-c immobilised on C_{15}-SAM-coated electrodes. The black (open circles), dark gray (open triangles), and light gray (solid squares) symbols refer to the data obtained from an Ag (TR SERR), Au–SAM–Ag (TR SERR), and Au electrode (rapid-scan SEIRA) (Table 2). The solid line represents a fit of Eq. (5) to the experimental data for the Ag electrode, taken from Ref. [27], whereas in the case of Au and Au–SAM–Ag, dotted lines are included to guide the eyes. Further details of the experiments and the data analysis are given in the text.

We now consider the overpotential-dependence of k_{ET} determined for Cyt-c on C_{15}-SAM-coated Au and Au–SAM–Ag hybrid electrodes, determined by rapid-scan SEIRA and TR SERR spectroscopy, respectively. In both cases, k_{ET} displays a drastically weaker increase with increasing $|\eta|$ (Fig. 8). This discrepancy with respect to Ag can hardly be rationalised on the basis of Eq. (5) since it would imply a physically meaningless low value for reorganisation energy, specifically for the SAM-coated Au electrode. Instead, in a first approximation, one may expect that λ should be similar for Cyt-c, independent of the kind of the supporting metal (*vide infra*).

The crucial electrochemical property that is different for SAM-coated Au and Ag electrodes is the potential of zero-charge E_{pzc}. This quantity depends of the crystalline structure of the metal and the type of SAM-coating and has been determined to be –0.45 and –0.2 V for C_{10}-SAM-coated Ag and Au–SAM–Ag electrodes [50]. It is reasonable to assume that the values for the respective C_{15}-coated electrodes are very similar [66]. Correspondingly, we assume $E_{pzc} = -0.05$ V for C_{15}-SAM-coated Au electrodes taking into account literature data [66]. The difference between the actual electrode potential E and E_{pzc} is proportional to the electric field in the SAM/Cyt-c interface [26,54]. Thus, the ET reactions of Cyt-c at Au and Ag electrodes take place under the action of opposite electric fields, and moreover, experience increasing field strengths for Au but decreasing strengths for Ag upon increasing the driving force for reduction, i.e. with increasingly negative overpotential $\eta = E - E^0$, taking into account the redox potentials of −0.01 V and +0.04 V for Cyt-c on C_{15}-SAM-coated Ag and Au electrodes, respectively [12,13]. Accordingly, the electric field variation for the Au–SAM–Ag electrode lies in between those for the Ag and Au electrode as it first decreases until $E = E^0$ ($E^0 = +0.04$ V [50]) and then increases again for $E < E_{pzc}$.

As shown previously for the charge recombination in photosynthetic systems, ET transfer reactions may be accelerated or slowed down by an externally applied electric field (e.g. [67–69]). These and related experimental data have been attributed to an electric-field dependent variation of the free-energy term of the Marcus equation [67,70], as the electric-field dependence of the electronic parameter is usually very small [71]. Accordingly, we have adopted these approximations and used a simple electric-field dependent correction to the free-energy term to rationalise

the present kinetic data. These approximations imply that, due to the fast protein re-orientation at C_{15}-SAM coatings (*vide supra*), any electric-field dependent differences in the orientational distribution of the immobilised Cyt-c on the three electrode systems have no effect on the ET kinetics, i.e. ET always takes place via the optimum electron coupling.

Assuming a linear relationship between E_{pzc} and the electric field strength [26,54], the actual driving force may be given by an effective overpotential η_{eff} according to Eq. (6)

$$\eta_{eff} = \eta + [a_0 + a_1 \cdot (E - E_{pzc})] = (E - E^0) + [a_0 + a_1 \cdot (E - E_{pzc})] \quad (6)$$

where a_0 and a_1 are constants. Then Eq. (5) is modified to

$$\frac{k_{ET}(E)}{k_{ET}(0)} = \frac{erfc\left(\frac{\lambda + e(E-E^0) + e[a_0 + a_1(E-E_{pzc})]}{\sqrt{4\lambda k_B T}}\right)}{erfc\left(\frac{\lambda + e[a_0 + a_1(E^0 - E_{pzc})]}{\sqrt{4\lambda k_B T}}\right)} \quad (7)$$

Eq. (7) is then fitted to the experimental data for C_{15}-SAM-coated Ag and Au–SAM–Ag electrodes setting $\lambda = 0.22$ eV [27] in both cases and using the experimentally determined redox potentials of −0.01 and +0.04 V for Cyt-c on C_{15}-SAM-coated Ag and Au–SAM–Ag electrodes, respectively [26,50]. Thus, a good and consistent description is achieved with the same value for a_1 (ca. 0.01) and a_0 of ca. −0.004 and −0.04 V for Ag and Au–SAM–Ag, respectively (Fig. 9). With these parameters, the ratio of the ET rate constants at zero-driving force for Cyt-c at C_{15}-SAM-coated Ag and Au–SAM–Ag, $k_{ET}(0, Ag)/k_{ET}(0, AuAg)$, is calculated to be ca. 0.4 which is in qualitative agreement with the experimental value of 0.2 (Table 2).

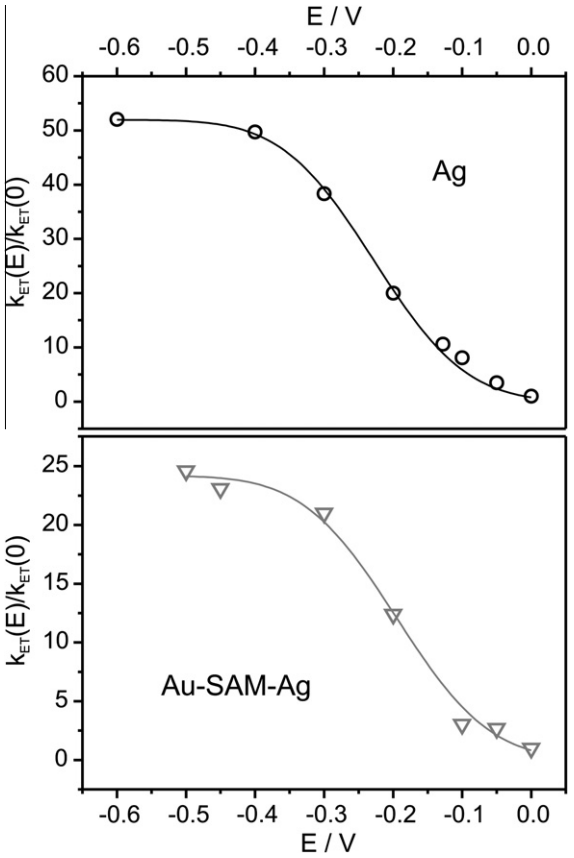

Fig. 9. Potential-dependence of the heterogeneous electron transfer rate constant k_{ET} for Cyt-c immobilised on C_{15}-SAM-coated Ag (top) and Au–SAM–Ag (bottom) electrodes. The black (open circles) and dark gray (open triangles) symbols refer to the data obtained from a Ag and Au–SAM–Ag electrode, respectively. The solid lines represent fits of Eq. (7) to the experimental data. Further details of the experiments and the data analysis are given in the text.

The low number of experimental values for $k(\eta)$ of Cyt-c at the C_{15}-SAM-coated Au electrode does not justify a fit of Eq. (7) with two adjustable parameter but introducing the additional constraint of $k_{ET}(0, Ag)/k_{ET}(0, Au) = 0.5$ (Table 2), it turns out that a reasonable reproduction of the experimental data may be achieved by a similarly low value of a_0 as for Ag and Au–SAM–Ag but a distinctly more negative value for a_1.

Despite the crudeness of the present approach, the results allow concluding that electron tunnelling is controlled by the interfacial electric field. This electric-field dependence does not only account for the different overpotential-dependencies at the various electrodes. In addition, it provides a satisfactory explanation also for the different $k_{ET}(0)$ values although for this quantity, electrode-specific differences of ρ and V cannot be neglected *a priori*. However, the differences for the electronic densities of states ρ of the three electrode systems are expected to be relatively small [72,73] and, in particularly, cannot account for variations of $k_{ET}(0)$ by factor of more than 5. This is also true for the effect of the different tilt angles of the mercaptanes on Ag and Au surfaces [74–76], which in principle might alter the electronic coupling V. However, in particular the 2.5 larger $k_{ET}(0)$ for Au–SAM–Ag compared to Au argues against this interpretation. Thus, we conclude that also differences for $k_{ET}(0)$ at the various electrodes are largely due to the different interfacial electric fields.

Note that for all three electrodes, the parameter a_0 was found to be very small. Since this quantity can be considered a correction term for the reorganisation energy, it implies that λ is largely the same for all three systems and thus independent of the electric field (*vide supra*) [70]. A more specific and quantitative description of the electric-field effect, however, would require a more elaborate description of the interfacial electric field which is beyond the scope of the present work.

Extending this analysis to the overpotential measurements to C_{10}-SAM-coated electrodes (Table 2) is problematic due to the interferences of electron tunnelling with protein dynamics which for Ag has been shown to proceed on comparable time scales already at moderate overpotentials [42].

4.2. Protein re-orientation and reorganisation of the hydrogen bond network in the protein/SAM interface

At C_x-SAM coatings at Ag electrodes with $x \leqslant 5$, the interfacial ET is controlled by the orientational distribution and dynamics of the immobilised protein. In fact, the dynamics of the overall redox process is viscosity-dependent as reflected by the decrease of k_{relax} by a factor of 1.3 from the pure H_2O buffer to the sucrose containing solution at 1.2 cp. This decrease is the same for C_5-SAM and C_1-SAM coatings at the Ag electrode, implying that a potential electric-field dependence of the viscosity effect is beyond the detection limit.

Conversely, the decrease of k_{relax} induced by substituting H_2O against D_2O buffer varies with the thickness of the SAM. Whereas at C_5-SAM coatings on Ag electrodes $k_{relax}(H_2O)/k_{relax}(D_2O)$ is 1.3 and thus identical to the viscosity-induced decrease of the relaxation constant, the ratio increases to 2.5 at C_1-SAM coatings. Taking into account the intrinsically higher viscosity of D_2O buffer solution that corresponds to that of a H_2O buffer/sucrose solution at 1.2 cp, one may evaluate a true H/D kinetic isotope effect (KIE) at C_1-SAM coatings of ca. 2.0. At C_5-SAM coatings, however, the observed decrease of k_{relax} in D_2O appears to be largely a viscosity effect. An upper limit of the H/D KIE in that case, however, may be estimated to be 1.1, taking into account the experimental accuracy of the determination of k_{relax}. In this respect, the KIEs determined in this work are actually somewhat smaller than the previously reported values for which the viscosity contribution was not

considered [12]. For C_5-SAM-coated Au electrodes, TR SEIRA experiments reveal no viscosity dependence and no H/D KIE for k_{relax}, which in addition is distinctly larger ($800\ s^{-1}$) than for Ag. This finding indicates that at C_5-SAM-coated Au electrodes protein re-orientation is much faster than on the Ag electrode and does not appear to constitute the rate-limiting step of the interfacial redox process.

An increased viscosity is likely to slow-down the large-scale motions of the immobilised protein, specifically the change of the binding site via rotational diffusion [42,46]. However, also small-amplitude fluctuations of water molecules in the Cyt-c/SAM contact region are affected as concluded from recent studies on covalently attached Cyt-c that as well reveals a viscosity effect of k_{relax} in the non-tunnelling regime [47].

The molecular origin of the H/D KIE may be based on two different processes. First, the above-mentioned fluctuations of water molecules in the interface between Cyt-c and the SAM have been shown to be important for a fine adjustment of the protein orientation with respect to the surface and thus for a more efficient electronic coupling [46,48]. Such motions inevitably include a re-arrangement of the hydrogen bond network, which is part of the thermal fluctuations of the system and is not a pre-requisite for the ET although they may affect the rate of electron tunnelling. Second, the change of the charge distribution at the redox site associated with the ET requires a re-arrangement of the hydrogen bond network, specifically albeit not exclusively, in the immediate surroundings of the heme as a part of the structural reorganisation [12,27]. It might be that this process involves short-range proton translocations, corresponding to a proton-coupled electron transfer mechanism. Such a mechanism has been proposed in our previous study [12,27] and, recently, discussed in more detail by Davis and Waldeck [43] in the context of further experimental and theoretical data [30,77,78]. In any case, the fact that the same KIE is observed regardless of the H/D exchange method (*vide supra*) implies that the kinetically relevant protons are easily exchanged.

Both processes, the fluctuations of the hydrogen bond network in the Cyt-c/SAM interface, and the redox-linked re-arrangement of the internal hydrogen bond network, may account for the H/D KIE effects observed in this work. In each case, displacements of (partially) charged groups and protons are involved which are likely to be affected by the interfacial electric field. The decrease of the H/D-sensitive relaxation constant from C_5-SAMs to C_1-SAMs points to an electric-field dependent increase of the activation energy required for the underlying processes. Moreover, also the KIE itself increases with increasing field strength (i.e., from C_5- to C_1-SAMs).

4.3. Overall electric-field effect on the interfacial electron transfer process

Due to the electric-field dependent decrease of the protein re-orientation rate, the experimentally determined values for k_{orient} and k_{relax} are essentially the same for C_5-SAM-coated Ag electrodes [42]. Under these conditions, the interfacial redox process may be described by a convolution of protein re-orientation and orientation-dependent electron tunnelling probabilities [42,48]. Most likely, the majority of the proteins is bound to the SAM surface via the high affinity domain BD3 for which the average electronic coupling parameter is predicted to be lower by a factor of ca.10 as compared to the medium-affinity binding domain BD2 for which the largest average electron coupling parameter has been calculated [46]. As a consequence, electron tunnelling should be faster by a factor of 100 for Cyt-c bound via BD2 than via BD3. Thus, the lower limit for the heterogeneous ET rate (slow protein re-orientation) should be given by the average electron tunnelling rates via BD3 whereas the upper limit (fast protein re-orientation) results from electron tunnelling via BD2. Then, the upper limit of the ET rate at C_5-SAM coatings may be estimated on the basis of distance-dependent term in Eq. (4) by extrapolating the rate constants in the electron tunnelling regime (C_{15}- and C_{10}-SAMs) to the C_5-SAM system [12]. This leads to a limiting rate constant of $6 \times 10^5\ s^{-1}$ that is four orders of magnitude larger than the experimentally observed value for k_{relax}. This difference has to be compared with the gap of two orders of magnitude between the lower and upper limit for orientation-dependent tunnelling as derived from the MD simulations. Moreover, this discrepancy is even more severe considering the kinetics at the C_1-SAM since the experimental value for k_{relax} even drops compared to the C_5-SAM. Just due to the distance dependence one would have expected an increase of the rate constant by a factor ca. 500, independent of the protein orientation and orientational dynamics.

These considerations imply that with increasing electric field strength at short distances the electron tunnelling rate is drastically slowed down. Most likely, in this high-field regime, the electric-field dependence of the tunnelling rate is more complex than included in Eqs. (7) and (6). Specifically, the assumption of an electric-field independent electronic coupling parameter (Eq. (4)) might not be justified. In fact, the effect of the interfacial electric field on the electronic coupling parameter has not been considered in the previous calculations of the electron tunnelling probabilities for the various orientations of Cyt-c [46,48].

On the basis of this interpretation one can also understand the ca. 1000 times smaller relaxation constant for SAMs of the same length as C_{10} but which carry a phosphonate instead of a carboxylate head group [15]. Due to the significantly higher charge density on the phosphonate-terminated SAM, the interfacial electric field strength is larger than for the carboxyl-terminated SAM, causing the drastic decrease of the electron tunnelling rate constant. The same explanation holds for the ca. 40 times lower k_{ET} at Ag electrodes covered with sulphate anions compared to the C_1-coated Ag electrode [58].

The interfacial redox process of Cyt-c on electrodes involves four different elementary steps, that are electron tunnelling coupled with the reorganisation of the protein structure, protein re-orientation on the SAM surface, and the re-arrangement of the hydrogen bond network in the protein/SAM interface and possibly also inside the protein. The individual steps depend on the local electric field, which in turn is controlled by the distance- and potential-dependence of the surface charge density on the SAM σ_S and of the quantity $(E - E_{pzc})$ [26,54]. The interplay of these electric-field dependent steps results in a complex overall potential- and distance-dependent kinetic behaviour.

Since the surface change density σ_S and $(E - E_{pzc})$ are different for different metals (i.e. Ag and Au) and the different types of coatings (i.e., charged, polar, or hydrophobic SAM surfaces) one may readily understand why the experimentally determined rate constants may differ among the various electrode/SAM systems but display, *in toto*, a similarly shaped distance-dependence [12,15,23,25,29–32,36]. At C_5-SAM-coated Au electrodes, for instance, k_{relax} at zero-driving force ($E = E^0$) is more than 6 times larger than in the case of Ag. This difference can be attributed to the fact that $|E^0 - E_{pzc}|$ is smaller for Au and, hence, also the electric field is weaker for Au than for Ag (*vide supra*) such that both electronic tunnelling and, as supported by the lack of a significant viscosity and H/D KIE effect, also protein re-orientation and hydrogen bond fluctuations are faster. On the other hand, an electrochemical investigation by Davis and Waldeck [43] reported a viscosity-corrected H/D KIE of ca. 1.2 for Cyt-c immobilised on Au electrodes coated by mixed carboxyl- and hydroxyl-terminated SAMs of 5 and 4 methylene groups, respectively. This difference compared to the present results is evidently due to the mixed monolayer that, compared to the pure carboxyl-terminated SAM used in this work,

affords a ca. 6 times larger k_{relax}, close to the rate constants of the viscosity- and H/D-dependent processes.

5. Conclusions

We have shown that the electric-field effects on protein motion, electron tunnelling, and hydrogen bond re-arrangements provide the basis for a consistent description of the present and previous experimental findings on the heterogeneous ET reaction of Cyt-c obtained for different electrode systems and SAM-coatings [12,15,23,25,29–32,36]. Moreover, these electric-field effects seem to constitute a general mechanism for interfacial processes of quite different redox proteins, since in each case the same elementary steps are involved. Details may be different depending on the surface charge of the protein's binding domains that may be either cationic, anionic, or hydrophobic and may contain heme or copper redox centers [51–55].

Acknowledgement

The work was supported by the DFG (Cluster of Excellence – UniCat).

References

[1] J.Ó.M. Bockris, A.K.N. Reddy, M. Gamboa-Aldeco, Modern Electrochemistry, vol. 2A, Kluwer, Academic, New York, 2000.
[2] J.Ó.M. Bockris, A.K.N. Reddy, Modern Electrochemistry, vol. 2B, Kluwer Academic, New York, 2000.
[3] A.M. Kuznetsov, J. Ulstrup, Electron Transfer in Chemistry and Biology an Introduction to the Theory, Wiley-VCH, Weinheim, 1998.
[4] O. Hammerich, J. Ulstrup, Bioinorganic Electrochemistry, Springer, New York, 2008.
[5] A.J. Bard, L.R. Faulkner, Electrochemical Methods: Fundamentals and Applications, Dekker, New York, 2000.
[6] F.A. Armstrong, Curr. Opin. Chem. Biol. 9 (2005) 110.
[7] K. Kneipp, M. Moskovits, H. Kneipp (Eds.), Surface-enhanced Raman Scattering: Physics and Applications, Springer, Berlin, 2006.
[8] F. Siebert, P. Hildebrandt, Vibrational Spectroscopy in Life Science, Wiley-VCH, Weinheim, 2007.
[9] S. Lecomte, H. Wackerbarth, T. Soulimane, G. Buse, P. Hildebrandt, J. Am. Chem. Soc. 120 (1998) 7381.
[10] H. Wackerbarth, U. Klar, W. Günther, P. Hildebrandt, Appl. Spectrosc. 53 (1999) 283.
[11] D.H. Murgida, P. Hildebrandt, Angew. Chem. Int. Ed. 40 (2001) 728.
[12] D.H. Murgida, P. Hildebrandt, J. Am. Chem. Soc. 123 (2001) 4062.
[13] N. Wisitruangsakul, I. Zebger, K.H. Ly, D.H. Murgida, S. Egkasit, P. Hildebrandt, Phys. Chem. Chem. Phys. 10 (2008) 5276.
[14] D.H. Murgida, P. Hildebrandt, Chem. Soc. Rev. 37 (2008) 937.
[15] D.H. Murgida, P. Hildebrandt, Phys. Chem. Chem. Phys. 7 (2005) 3773.
[16] K. Ataka, J. Heberle, J. Am. Chem. Soc. 126 (2004) 9445.
[17] K. Ataka, J. Heberle, Anal. Bioanal. Chem. 388 (2007) 47.
[18] R.G. Nuzzo, D.L. Allara, J. Am. Chem. Soc. 105 (1983) 4481.
[19] L.K. Prime, G.M. Whitesides, Science 252 (1991) 1164.
[20] M.J. Tarlov, E.F. Bowden, J. Am. Chem. Soc. 113 (1991) 1847.
[21] S. Song, R.A. Clark, E.F. Bowden, M.J. Tarlov, J. Phys. Chem. 97 (1997) 6564.
[22] T.M. Nahir, R.A. Clark, E.F. Bowden, Anal. Chem. 66 (1994) 2595.
[23] Z.Q. Feng, S. Imabayashi, T. Kakiuchi, K. Niki, J. Chem. Soc. Faraday Trans. 93 (1997) 1367.
[24] A. El Kasmi, J.M. Wallace, E.F. Bowden, S.M. Binet, R.J. Linderman, J. Am. Chem. Soc. 120 (1998) 225.
[25] A. Avila, B.W. Gregory, K. Niki, T.M. Cotton, J. Phys. Chem. B 104 (2000) 2759.
[26] D.H. Murgida, P. Hildebrandt, J. Phys. Chem. B 105 (2001) 1578.
[27] D.H. Murgida, P. Hildebrandt, J. Phys. Chem. B 106 (2002) 12814.
[28] C.E. Nordgren, D.J. Tobias, M.L. Klein, J.K. Blasie, Biophys. J. 83 (2002) 2906.
[29] K. Niki, W.R. Hardy, M.G. Hill, H. Li, J.R. Sprinkle, E. Margoliash, K. Fujita, R. Tanimura, N. Nakamura, H. Ohno, J.H. Richards, H.B. Gray, J. Phys. Chem. B 107 (2003) 9947.
[30] D.E. Khoshtariya, J.J. Wei, H.Y. Liu, H.J. Yue, D.H. Waldeck, J. Am. Chem. Soc. 125 (2003) 7704.
[31] D.H. Murgida, P. Hildebrandt, J. Wei, Y.F. He, H.Y. Liu, D.H. Waldeck, J. Phys. Chem. B 108 (2004) 2261.
[32] J.J. Wei, H.Y. Liu, K. Niki, E. Margoliash, D.H. Waldeck, J. Phys. Chem. B 108 (2004) 16912.
[33] J. Petrovic, R.A. Clark, H.J. Yue, D.H. Waldeck, E.F. Bowden, Langmuir 21 (2005) 6308.
[34] H.J. Yue, D.H. Waldeck, Curr. Opin. Solid State Mater. Sci. 9 (2005) 28.
[35] J.S. Xu, E.F. Bowden, J. Am. Chem. Soc. 128 (2006) 6813.
[36] H.J. Yue, D. Khoshtariya, D.H. Waldeck, J. Grochol, P. Hildebrandt, D.H. Murgida, J. Phys. Chem. B 110 (2006) 19906.
[37] K.B. Holt, Langmuir 22 (2006) 4298.
[38] M.T. de Groot, M. Merkx, M.T.M. Koper, Langmuir 23 (2007) 3832.
[39] X.U. Jiang, K. Ataka, J. Heberle, J. Phys. Chem. C 112 (2008) 813.
[40] K.L. Davis, B.J. Drews, H. Yue, D.H. Waldeck, K. Knorr, R.A. Clark, J. Phys. Chem. C 112 (2008) 6571.
[41] J.J. Feng, D.H. Murgida, T. Utesch, M.A. Mroginski, P. Hildebrandt, I. Weidinger, J. Phys. Chem. B 112 (2008) 15202.
[42] A. Kranich, H.K. Ly, P. Hildebrandt, D.H. Murgida, J. Am. Chem. Soc. 130 (2008) 9844.
[43] K.L. Davis, D.H. Waldeck, J. Phys. Chem. B 112 (2008) 12498.
[44] D. Millo, A. Ranieri, P. Gross, M. Borsari, H.K. Ly, P. Hildebrandt, G.J.L. Wuite, C. Gooijer, G. van der Zwan, J. Phys. Chem. C 113 (2009) 2861.
[45] J.J. Feng, U. Gernert, M. Sezer, U. Kuhlmann, D.H. Murgida, C. David, M. Richter, A. Knorr, P. Hildebrandt, I. Weidinger, Nano Lett. 9 (2009) 298.
[46] D.A. Paggi, D.F. Martín, A. Kranich, P. Hildebrandt, M. Martí, D.H. Murgida, Electrochim. Acta 54 (2009) 4963.
[47] H.K. Ly, M. Marti, D.F. Martin, D.A. Paggi, W. Meister, A. Kranich, I.M. Weidinger, P. Hildebrandt, D.H. Murgida, Chem. Phys. Chem. 11 (2010) 1225.
[48] D.A. Paggi, D.F. Martín, P.M. Biase, P. Hildebrandt, M.A. Martí, D.H. Murgida, J. Am. Chem. Soc. 132 (2010) 5769.
[49] S. Georg, J. Kabuss, I.M. Weidinger, D.H. Murgida, P. Hildebrandt, A. Knorr, M. Richter, Phys. Rev. E 81 (2010) 046101.
[50] M. Sezer, J.J. Feng, H.K. Ly, Y. Shen, T. Nakanishi, U. Kuhlmann, H. Möhwald, P. Hildebrandt, I. Weidinger, Phys. Chem. Chem. Phys. 12 (2010) 9822.
[51] J.Q. Chi, J.D. Zhang, J.E.T. Andersen, J. Ulstrup, J. Phys. Chem. B 105 (2001) 4669.
[52] K. Fujita, N. Nakamura, H. Ohno, B.S. Leigh, K. Niki, H.B. Gray, J.H. Richards, J. Am. Chem. Soc. 126 (2004) 13954.
[53] A. Kranich, H. Naumann, F.P. Molina-Heredia, H.J. Moore, T.R. Lee, S. Lecomte, M.A. de la Rosa, P. Hildebrandt, D.H. Murgida, Phys. Chem. Chem. Phys. 11 (2009) 7390.
[54] P. Zuo, T. Albrecht, P.D. Barker, D.H. Murgida, P. Hildebrandt, Phys. Chem. Chem. Phys 11 (2009) 7430.
[55] M.L. Vargo, C.P. Gulka, J.K. Gerig, C.M. Manieri, J.D. Dattelbaum, C.B. Masrks, N.T. Lawrence, M.L. Trawick, M.C. Leopold, Langmuir 26 (2010) 560.
[56] S. Döpner, P. Hildebrandt, A.G. Mauk, H. Lenk, W. Stempfle, Spectrochim. Acta A – Mol. Biomol. Spectrosc. 52 (1996) 573.
[57] S. Oellerich, H. Wackerbarth, P. Hildebrandt, J. Phys. Chem. B 106 (2002) 6566.
[58] H. Wackerbarth, P. Hildebrandt, Chem. Phys. Chem. 4 (2003) 714.
[59] P.M. De Biase, D.A. Paggi, F. Doctorovich, P. Hildebrandt, D.A. Estrin, D.H. Murgida, M.A. Marti, J. Am. Chem. Soc. 131 (2009) 16248.
[60] L. Rivas, D.H. Murgida, P. Hildebrandt, J. Phys. Chem. B 106 (2002) 4823.
[61] L. Mayne, Y. Patterson, D. Cesaroli, S.W. Englander, Biochemistry 31 (1992) 10678.
[62] S. Döpner, P. Hildebrandt, G.E. Heibel, F. Vanhecke, A.G. Mauk, J. Mol. Struct. 349 (1995) 125.
[63] J.E. Kim, M.A. Pribisko, H.B. Gray, J.R. Winkler, Inorg. Chem. 43 (2004) 7953.
[64] R.A. Marcus, J. Chem. Phys. 43 (1965) 679.
[65] C.E.D. Chidsey, Science 251 (1991) 919.
[66] P. Ramirez, R. Andreu, A. Cuesta, C.J. Calzado, J.J. Calvente, Anal. Chem. 79 (2007) 6473.
[67] D.J. Lockhart, C. Kirmaier, D. Holten, S.G. Boxer, J. Phys. Chem. 94 (1990) 6987.
[68] K. Lao, S. Franzen, M. Steffen, D. Lambright, R. Stanley, S.G. Boxer, Chem. Phys. 197 (1995) 259.
[69] M. Bixon, J. Jortner, J. Phys. Chem. 92 (1989) 7148.
[70] K. Seki, Traytak, M. Tachiya, J. Chem. Phys. 118 (2003) 679.
[71] S.H. Lin, C.Y. Yeh, G.Y.C. Wu, Chem. Phys. Lett. 166 (1990) 195.
[72] R.J. Forster, P. Loughman, T.E. Keyes, J. Am. Chem. Soc. 122 (2000) 11948.
[73] R.R. Ford, J. Pritchard, Trans. Faraday Soc. 67 (1971) 216.
[74] J.C. Love, L.A. Estroff, J.K. Kriebel, R.G. Nuzzo, G.M. Whitesides, Chem. Rev. 105 (2005) 1103.
[75] P.E. Laibinis, G.M. Whitesides, D.L. Allara, Y.T. Tao, A.N. Parikh, R.G. Nuzzo, J. Am. Chem. Soc. 113 (1991) 7152.
[76] C.D. Bain, E.B. Troughton, Y.T. Tao, J. Evall, G.M. Whitesides, R.G. Nuzzo, J. Am. Chem. Soc. 111 (1989) 321.
[77] S.A. Kang, K.R. Hoke, B.R. Crane, J. Am. Chem. Soc. 128 (2006) 2346.
[78] H. Decornez, S. Hammes-Schiffer, J. Phys. Chem. A 104 (2000) 9370.